Materials & Design 209 (2021) 109970

Contents lists available at ScienceDirect

Materials & Design

journal homepage: www.elsevier.com/locate/matdes

Direct observation of nanocrystal-induced enhancement of tensile ductility in a metallic glass composite

Christoph Gammer [a,*], Christian Rentenberger [b], Denise Beitelschmidt [c,1], Andrew M. Minor [d], Jürgen Eckert [a,e]

[a] Erich Schmid Institute of Materials Science, Austrian Academy of Sciences, Jahnstraße 12, 8700 Leoben, Austria
[b] University of Vienna, Faculty of Physics, Physics of Nanostructured Materials, Boltzmanngasse 5, 1090 Wien, Austria
[c] Leibniz Institute for Solid State and Materials Research (IFW) Dresden e.V., Helmholtzstr. 20, 01069, Dresden, Germany
[d] Department of Materials Science and Engineering, University of California, Berkeley and National Center for Electron Microscopy, Molecular Foundry, Lawrence Berkeley National Laboratory, Berkeley, USA
[e] Department Materials Science, Chair of Materials Physics, Montanuniversität Leoben, Jahnstrasse 12, 8700 Leoben, Austria

HIGHLIGHTS

- A combination of elastodynamic deformation and heating was used to make a metallic glass nanocomposite.
- Homogenous precipitation of mondisperse round nanocrystals (20 nm) with an average spacing of only 150 nm is achieved.
- In situ tensile testing is carried out in a transmission electron microscope.
- While the monolithic glass shows catastrophic fracture, the shear band is stopped in the nanocomposite.

GRAPHICAL ABSTRACT

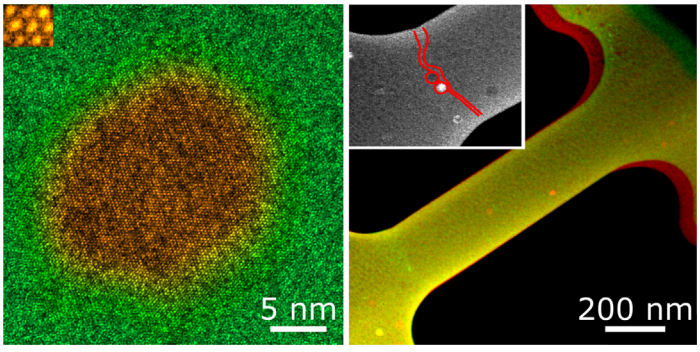

ARTICLE INFO

Article history:
Received 20 April 2021
Revised 23 June 2021
Accepted 6 July 2021
Available online 7 July 2021

Keywords:
Metallic glass
Nanocrystals
Transmission electron microscopy
In situ deformation

ABSTRACT

Bulk metallic glasses (BMGs) have attracted wide interest, but their successful application is hindered by their low ductility at room temperature. Therefore, the use of composites of a BMG matrix with crystalline secondary phases has been proposed to overcome this drawback. In the present work we demonstrate the fabrication of a tailored BMG nanocomposite containing a high density of monodisperse nanocrystals with a size of around 20 nm using a combination of mechanical and thermal treatment of $Cu_{36}Zr_{48}Al_8Ag_8$ well below the crystallization temperature. Direct observations of the interaction of the nanocrystals with a shear band during *in situ* deformation in a transmission electron microscope demonstrate that the achieved nanocomposite has the potential to inhibit catastrophic fracture in tension. This demonstrates that a sufficient number of nanoscale structural heterogeneities can be a route towards BMG composites with superior mechanical properties.

1. Introduction

Due to their structural disorder and thus absence of crystallographic features such as dislocations, bulk metallic glasses (BMGs) show desirable properties such as high strength, good wear and

* Corresponding author.
E-mail address: christoph.gammer@oeaw.ac.at (C. Gammer).
[1] Present address: ZwickRoell GmbH&Co.KG, August-Nagel-Str. 11, 89079 Ulm, Germany.

https://doi.org/10.1016/j.matdes.2021.109970
0264-1275/

corrosion resistance and good formability [1–3]. Their unique functional properties make metallic glasses attractive materials for applications as magnetic, electrocatalytic materials or for microelectromechanical systems [4,5]. To achieve room temperature plasticity in BMGs great efforts are undertaken e.g. by rejuvenation of the structure [6,7]. Still, extended tensile ductility in monolithic BMGs has to date been demonstrated only for sample sizes below around 100 nm [8–10]. Therefore, ductile BMG composites with a glassy matrix and crystalline secondary phases have attracted wide interest for the flexibility they represent for amorphous alloy design [11–14]. Under compression a significantly improved ductility was found for various composite materials. Increasing the crystalline volume fraction leads to an increase in the tensile ductility at the expense of strength and hardness [11,12]. In addition, efforts have been made to design BMGs with nanoscale heterogeneities. For example, phase-separated BMGs containing different glassy-phase structures were shown to exhibit large room-temperature plasticity [15]. For some BMGs *in situ* crystallization during deformation can lead to the formation of nanocrystals and they can have a positive effect on the mechanical properties [16,17] and it was even demonstrated that some ductility in tension can be achieved without loss of hardness [17]. Similarly, heterogeneities in the form of complex stress distributions have been shown to enhance the tensile ductility [18,19]. Moreover, nanolaminates with alternating layers of crystalline and amorphous materials have demonstrated good mechanical properties [20,21]. Finally, porous structures or nanolattices can be used as a way to suppress brittle failure [22,23]. In the present work the effect of nanosized crystallites on the mechanical properties of a BMG is analyzed. For this purpose, a CuZr-based BMG nanocomposite containing a large density of homogeneously distributed mono-disperse nanocrystals is produced and their effect on the deformation behavior is studied by *in situ* deformation experiments within the transmission electron microscope (TEM).

2. Materials and methods

$Cu_{36}Zr_{48}Al_8Ag_8$ ingots were prepared by arc-melting of high-purity elements (Al, Cu: 99.99 wt%, Ag: 99.9 wt% Zr: 99.8 wt%) under a Ti-gettered Ar atmosphere. From the ingots, BMG plates (75 × 10 × 1.5 mm) were cast into Cu-molds by suction-casting (modified Bühler MAM1). To make the BMG nanocomposites, BMG stripes were ground down to a thickness of 0.8 mm and dynamically loaded in a Netsch DMA 242C dynamical mechanical analyzer (DMA). A detailed schematic of the setup is given in the Supplementary Figure S1. Loading was carried out in 3-point bending mode at 1 Hz with a force of 6.1 N and an amplitude of 10 μm. This results in a maximum stress of about 26 MPa, being in the elastic regime. At the same time the samples were heated at a rate of 2 K/min up to 623 K. It should be pointed out that this temperature is well below the crystallization temperature T_x = 783 K and below the glass transition temperature T_g = 709 K, measured by differential thermal analysis using a heating rate of 20 K/min. To analyze the microstructure of the samples a TEM lamella was extracted from the specimen using a Zeiss Crossbeam 1540 XB focused ion beam system (FIB) system and thinned to electron transparency. In addition to TEM and scanning TEM (STEM) investigations including diffraction, aberration-corrected high-resolution TEM (HRTEM) imaging was carried out. The micro-tensile specimens for *in situ* TEM deformation were prepared in a FEI Strata 235 FIB/SEM equipped with an Omniprobe micromanipulator. Rectangles (about 8 × 2 μm in size) were cut from the TEM lamella and transferred to a Hysitron Push-to-Pull device (PTP), that transforms the compressive motion of an indenter into a tensile test. The samples were attached to the device using a Pt-deposition system and cut into a miniaturized dogbone specimens. In situ TEM tensile testing was carried out in displacement control using a Hysitron PI95 Picoindenter at a strain rate of 0.233 nm/s. Load-displacement curves were recorded during deformation. The load–displacement curves were converted into engineering stress–strain curves using the measured dimensions of the tensile bars. The maximum elongation of the tensile bar before fracture was determined by measuring the true elongation measured in the *in situ* TEM video. The ratio of the true elongation and the elongation measured by the Picoindenter was used to correct for errors due to the stiffness of the testing setup.

3. Results

Fig. 1a shows a typical TEM image and diffraction pattern from the as-cast CuZrAlAg BMG specimen revealing a homogenous glassy structure, without any sign of nanocrystals or phase separation. To test the mechanical properties of the monolithic CuZrAlAg BMG specimen, tensile tests were performed in the TEM using a Hysitron PI95 indentation holder. Deformation was carried out in displacement control using a dog-bone-shaped specimen with a dimension of 1000x200 nm and a thickness of 200 nm mounted on a Hysitron PTP device [24]. Fig. 1b shows the resulting stress–strain curve. The stress–strain curve is characteristic for monolithic BMGs, showing a high yield strength close to the theoretical limit and large elastic strain limit, but brittle fracture without any sign of ductility. A video was recorded during deformation in TEM bright-field mode (see Supplementary Materials). Fig. 1c shows three frames extracted from the video. The direct comparison of the initial and deformed state clearly shows the elastic elongation. After elongation the sample fractures abruptly with a single catastrophic shear band. The test clearly demonstrates, that monolithic BMGs fracture catastrophically in tension, as there is no mechanism to stop the shear band once formed. The limited tensile ductility poses a significant limitation for the successful use of BMGs.

Therefore, to inhibit catastrophic fracture, it is the aim to create a BMG composite with tailored nanoscale structural heterogeneities. To achieve a composite with well-dispersed, densely spaced and small nanocrystals, the samples were heated to a temperature of 623 K, well below the crystallization temperature. During heating, dynamical mechanical loading was carried out in the elastic regime in three-point bending. The loading was carried out at 80% of the maximum elastic stress. Fig. 2a shows an annular dark-field (ADF) STEM image of the nanocomposite achieved through the combination of heating with dynamical mechanical loading. Due to their crystalline nature the nanocrystals show bright or dark-contrast depending on their orientation with respect to the electron beam. Inspection of the morphology, size and distribution of the individual nanocrystals formed through the combination of mechanical and thermal treatment, reveals that they all have a similar size, round shape and are homogeneously dispersed in the glassy matrix. They show a narrow size distribution of 22 ± 5 nm (a detailed histogram is given in Fig. 2d). Fig. 2b shows a high-resolution TEM (HRTEM) image of an individual nanocrystal. The crystal is surrounded by the glass matrix. The nanocrystal is spherical and shows the Al_2Zr crystal structure and the glass matrix exhibits no signs of crystalline order. The interface between crystal and glass matrix is well-defined. For better visibility the image is colorized according to the crystalline order. As a measure of the crystalline order, we computed and smoothed a Fourier-filtered image by masking in the FFT all crystalline spots but excluding the forward scattered beam. The magnified inset in Fig. 2b clearly demonstrates the regular crystal structure of the nanocrystal. Close inspection of the nanocrystal confirms that is defect-free and has a well-defined crystal structure.

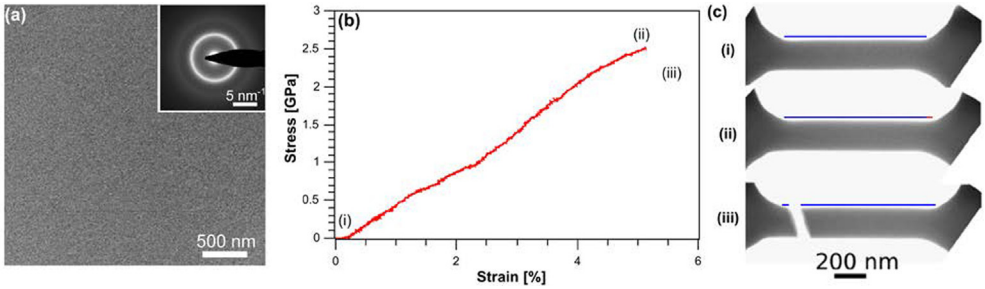

Fig. 1. Structure and mechanical properties of the monolithic CuZrAlAg BMG. (a) TEM bright-field image revealing the homogenous glassy structure. The amorphous structure is also confirmed in the corresponding electron diffraction pattern shown as inset. To study the mechanical properties an *in situ* tensile is carried out in the TEM. (b) The engineering stress–strain curve reveals elastic elongation followed by brittle fracture, without any sign of ductility. (c) Three frames were extracted from the video acquired in TEM bright-field mode during deformation corresponding to (i) the initial state, (ii) the elongated state and (iii) the sample after fracture; their time step is indicated in the load–displacement curve. To visualize the elongation of the gauge section, the initial length is shown in blue and the elongation in red. The result clearly demonstrates the brittle nature of the monolithic BMG lacking a mechanism to stop the catastrophic shear band. (For interpretation of the references to color in this figure legend, the reader is referred to the web version of this article.)

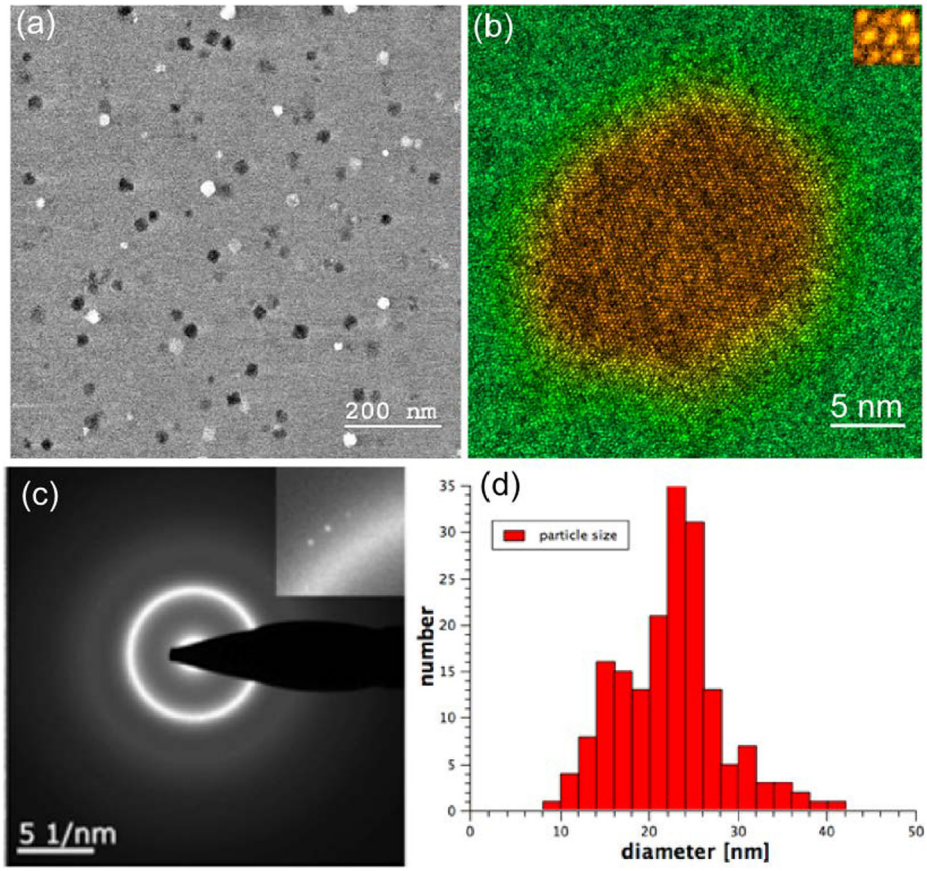

Fig. 2. Microstructure of the CuZrAlAg BMG nanocomposite. (a) Annular dark-field STEM image revealing homogeneously distributed nanocrystals in the amorphous matrix. The nanocrystals are round and have a narrow size distribution of 22 ± 5 nm, as shown in the histogram (b). (c) Color-coded high-resolution TEM image of an individual nanocrystal (green = amorphous, red = crystalline) showing a Al_2Zr crystal. For better visibility the crystal structure is magnified by a factor of 5 in the inset. (d) The electron diffraction pattern shows crystalline reflections and a broad halo from the amorphous matrix. A portion of the pattern is magnified in the inset to better reveal the spots from the nanocrystals. (For interpretation of the references to color in this figure legend, the reader is referred to the web version of this article.)

To analyze the crystal structure of the nanocrystals in more detail, a combination of electron diffraction (see Fig. 2c) and HRTEM imaging were used, revealing that the nanocrystals can have multiple different crystal structures. The encountered crystal structures include Cu_2Zr (cF16), Al_2Zr (hP12), AlCuZr (cF24) and $Al_{2.5}Cu_{0.5}Zr$ (cP4), similar to the phases observed after annealing [25]. A detailed analysis is given in Supplementary Figure S2. In addition, chemical analysis of the nanocrystals was carried out using energy-dispersive X-ray spectroscopy (EDS), showing a chemical difference between the nanocrystals and the glassy matrix. An EDS map of a nanocrystal revealing an increase of Al and a decrease in Ag compared with the matrix is shown in Supplementary Materials Figure S1a. The difference in chemical composition between the nanocrystals and the amorphous matrix was also confirmed using high-angle annular dark-field (HAADF) STEM imaging showing that the nanocrystals have a lower atomic number than the matrix (see Supplementary Materials Figure S3b). This is in good accordance with the Al-rich phases. Few nanocrystals

show only a small contrast difference to the matrix which can be attributed to Cu_2Zr.

To compare the mechanical properties of the nanocomposite to those of the monolithic BMG, tensile tests were performed *in situ* in the TEM. Deformation was carried out in displacement control using a dog-bone-shaped specimen with a dimension of 800x300 nm and a thickness of 85 nm. Fig. 3a displays the load–displacement curve obtained during the *in situ* test. The curve shows an initial elastic regime that is characterized by a rather linear stress increase, followed by an abrupt load drop. The load drop stems from a sudden elongation of the specimen due to the formation of a shear band. The experiment was carried out in displacement control controlled by a 78 kHz feedback loop. Therefore, the large slip from the shear band causes a sudden elongation of the specimen leading to an extended stress drop. What is most striking is the fact that in contrast to the monolithic glass the shear banding event does not lead to catastrophic fracture and the sample continues to deform after the load drop. To correlate the mechanical data with the structural changes, a TEM dark-field video was recorded during the deformation test. The first halo (diffraction ring) of the amorphous structure was used as dark-field condition for the experiment. Fig. 3c-e show three frames extracted from the *in situ* TEM video. The full video is provided in the Supplementary Materials. The time steps of the extracted frames are indicated in the deformation curve with arrows (see Fig. 3a). Fig. 3c shows the dog-bone shaped tensile specimen before deformation. Some nanocrystals are visible exhibiting bright or dark contrasts depending on their orientation in the amorphous matrix. At the load drop the tensile specimen experiences a local slip event; however, the sample does not facture. To study the elongation of the sample due to the shear banding, the frames before and after the event were compared revealing a very large elongation of about 20 nm (the color overlay of the two frames is shown in Fig. 3b). The frame extracted after the load drop shows the traces of a shear band in the bottom left end of the tensile specimen, characterized by a brighter contrast (see Fig. 3d). Further deformation leads to final fracture (see Fig. 3e). It Is interesting to note that fracture is not observed at the location of the shear band, but at the other end of the gauge section. Shear banding and fracture close to the shoulder is in good agreement with the maximum stress location of the dogbone shaped specimen [26].

The inset in Fig. 3e shows a close-up of the location of the shear band recorded after the sample has fractured. For better visibility, the trace of the shear band and the interacting nanocrystals are marked. The shear band shows local deflection that coincides with the location of crystallites in the sample. The results indicate that the interaction of the shear band with the nanocrystals during deformation prevents final fracture. This unexpected behavior was confirmed in further tests showing similar behavior; the stress–strain curves for two additional tensile tests are given in Supplementary Figure S4. The direct comparison of the monolithic BMG specimen with the nanocomposite therefore clearly confirms the beneficial effect of the nanocrystals even for tensile deformation.

CuZrAlAg shows a very good glass-forming ability and a large supercooled liquid region, making it an attractive material for thermoplastic forming [27]. Minor compositional changes in CuZrAl (Ag) based BMGs can affect the glass-forming ability, the hidden order in the amorphous phase, as well as thermal stability and consequently crystallization [28,29]. The present results demonstrate

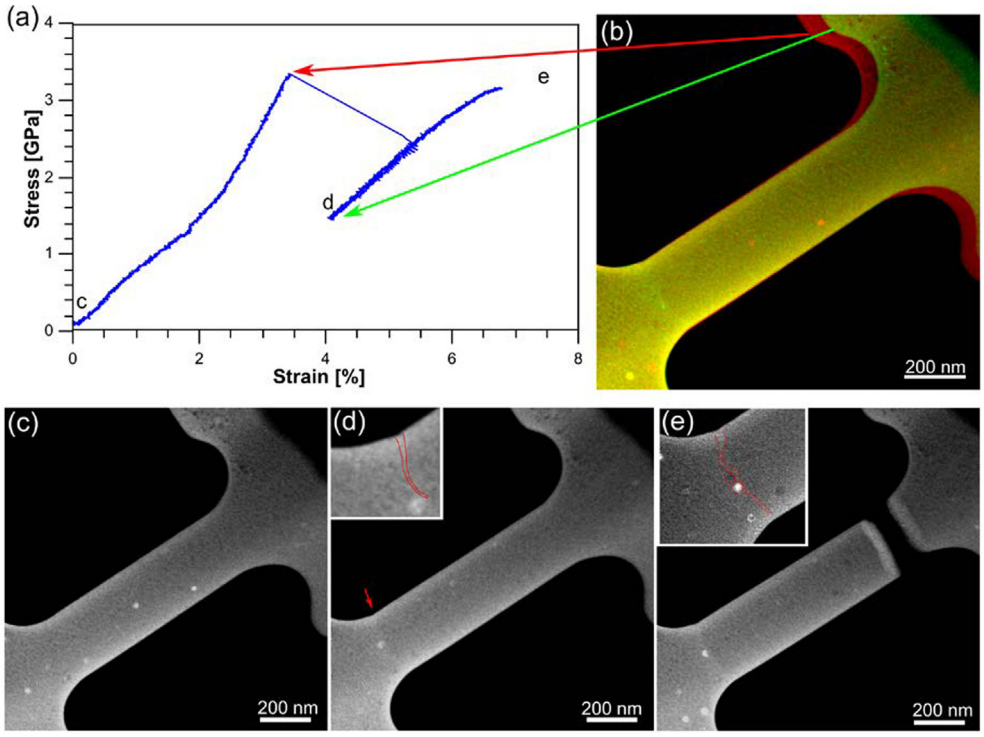

Fig. 3. In situ tensile test of the CuZrAlAg BMG nanocomposite. (a) Load-displacement curve, a major load drop is observed that does not lead to final fracture. To analyze the load-drop, a color overlay of two consecutive frames extracted from the video recorded in dark-field mode during *in situ* deformation is shown in (b). The direct comparison of the tensile specimen before (red) and after the load drop (green) reveals a significant elongation during the slip event. (c-e) Three frames were extracted from the video; their time step is indicated in the load–displacement curve. (c) Prior to deformation, some nanocrystals are visible. (d) A shear band is formed (see arrow) but does not lead to failure. The insert shows a zoom-in, where the shear step at the sample edge and the path of the shear band is indicated. (e) The sample continues to deform after the first shear band is formed and fractures at a different location. To study the mechanism inhibiting catastrophic fracture, a magnified image of the first shear band is shown in the inset, revealing the interaction of the nanocrystals with the shear band (indicated in red). (For interpretation of the references to color in this figure legend, the reader is referred to the web version of this article.)

the precipitation of evenly dispersed nanocrystals in $Cu_{36}Zr_{48}Al_8Ag_8$ through combined elastodynamic loading and heating up to 623 K. This temperature is significantly below the crystallization temperature (T_X) of 783 K. Studies of the crystallization behavior of CuZrAlAg metallic glass ribbons have shown that nanocrystals can be formed by annealing for 30 min at 743 K [25]. The nanocrystals formed during annealing exhibit similar phases to the nanocrystals observed in the present work (i.e. $AlCu_2Zr$, Al_2Zr and AgZr), but a less uniform distribution and larger size distribution [25]. Also, during cooling from the melt larger crystals are formed, corresponding to the $Cu_{10}Zr_7$ and the Zr_2Cu + $AlCu_2Zr$ eutectic phases [25,30]. Therefore, it can be concluded, that a combination of mechanical and thermal treatment significantly below the crystallization temperature is a promising approach for the formation of well-dispersed nanocrystals. In addition, the nanocrystals in the present BMG have a different composition to the surrounding matrix, further inhibiting excessive growth. The formation of a high number density of nanosized precipitates is of the fundamental constituent of crystalline high-performance alloys. Therefore, significant work has been performed to optimize and understand alloying and heat treatment approaches [31–34]. The present work demonstrates a strategy towards optimizing the number density and size distribution of crystalline precipitates in a BMG composite.

The *in situ* TEM experiments demonstrate that the interaction of the shear band with the nanocrystals prevents the sample from catastrophic fracture even under tension. Therefore, it can be concluded that a high number density of very small nanocrystalline precipitates is highly beneficial for the tensile deformation behavior. This effect is different to the ductility induced in MGs through sample size effects, that has attracted wide attention in literature [9,35]. A transition from brittleness to tensile ductility is observed when the sample size is reduced below some critical value, typically on the order of about 100 nm. This transition is caused by a change in deformation mechanism from shear band formation to necking with decreasing sample size [9,35]. The effects observed for the tension tests of the nanocomposite shown in the present work are different, revealing discrete shear events rather than homogenous deformation. The observed effect is also different to the ductility in BMGs induced by *in situ* crystallization or to the ductility induced by martensitic transformation of B2 precipitates [17,36]. In the present case, we have achieved a nanocomposite with a high number density of hard intermetallic nanocrystals. Therefore, it can be excluded that the yielding of the nanoparticles triggers a shear band and mainly two scenarios will occur during deformation. On the one hand the shear band can be triggered in the metallic glass matrix or sample surface or on the other hand it can be triggered by the nanocrystals acting as structural heterogeneity in the glass. It has been shown that the difference in elastic moduli between nanocrystals and matrix leads to stress concentration at the interface that activates rearrangements of the structure and the shear transformation zones (STZs) in the glassy phase [20,37,38]. The observation of the shear band following the nanocrystals demonstrates that the interaction of the stress around the shear band and around the crystals is crucial for the nucleation and propagation of the shear band. Due to the small spacing of the nanocrystals they can not only trigger local shear, but also interact with shear bands, leading to the observation of extended shear events without catastrophic fracture. The main factor affecting the tensile ductility is the spacing between the nanocrystals. If it is too large shear bands can pass though the glassy matrix resulting in early failure [39]. In the present case the spacing between the nanocrystals is only around 150 nm, making them effective barriers to the shear band propagation. Strikingly, due to the nanosize, this spacing is achieved while keeping the crystalline volume fraction at 2%, allowing to keep the high strength of the glassy matrix. This deformation mechanism is based on the internal spacing of the nanocrystals and therefore should be valid independent of sample size. In the case of an 85 nm thick specimen a single large shear event was observed and in the case of a 130 nm thick specimen multiple shear events have been encountered.

Serrated flow is typically observed during micro-compression experiments of metallic glasses reflecting discrete shear events. In microscale tensile deformation of monolithic BMG, a single shear band on the other hand leads to brittle failure (see Fig. 1). In the present case, however extended continued deformation was observed after the shear events demonstrating the ability of the nanocrystals to inhibit catastrophic fracture. The proliferation of soft sites by the electron beam during tensile in-situ experiments as observed recently [40] does not play a role in the present case since shear banding remains the dominant deformation mechanism and is clearly correlated with the presence of nanocrystals.

Multiple different approaches for designing BMG composites with crystalline precipitates have been discovered. The effect depends strongly on the size, volume fraction and dispersion of the crystalline phase [36]. An effective strategy to achieve ductile BMGs is the formation of a microstructure consisting of ductile crystalline dendrites embedded in a glassy matrix [41]. Still, an improvement of the mechanical properties can also achieved with brittle crystallites, providing that they do not percolate [42]. Experimental studies on the mechanisms responsible for the improved deformation properties of BMG composites are focused on post-mortem investigations [36,43]. Samples after fracture show a larger number of shorter shear bands in composites as compared to monolithic BMGs [36]. Molecular dynamics (MD) simulations of metallic glass composites with nanocrystalline precipitates have shown different possible mechanisms for the interaction of a shear band with a precipitate [44]. The arrangement of the heterogeneities is of great importance, as demonstrated by MD simulations of composites with pores [45]. The length-scale of the crystalline phase must match that of the shear bands to guarantee an effective interaction. The BMG composite achieved in the present study shows homogenously dispersed nanocrystals on a length-scale matching the shear band. In addition, the nanocrystals show intermetallic crystal structures exhibiting high hardness. Due to their small size, a small spacing can be reached even at a very low volume fraction of nanocrystals of a few percent, e.g. in the present case a volume fraction of 2 vol% and a spacing of 150 nm was estimated from the HAADF images. This enables to inhibit catastrophic fracture while retaining the beneficial properties of the BMG.

4. Conclusions

In summary, we have fabricated a BMG nanocomposite using a combination of mechanical and thermal treatment well below the crystallization temperature. The resulting specimens contain a large density of homogenously dispersed nanocrystals with a size of around 20 nm embedded in a glassy matrix. In contrast to conventional annealing treatments, the use of dynamic mechanical treatment during heating causes crystallization at lower temperatures and results in highly monodisperse round crystals. To test the effect of the nanocrystals on the mechanical behavior, *in situ* tensile tests in the TEM were carried out allowing to directly image the interaction of the nanocrystals with the shear bands. The tests show that the nanocrystals can inhibit catastrophic fracture in tension. This clearly demonstrates that tailored nanocomposites with well-dispersed crystals have the potential to improve the mechanical properties of BMGs. As the property improvement is based on the internal spacing of the nanocrystals, it is valid independent of

sample size. In crystalline high-performance alloys, the beneficial effect of small but densely spaced precipitates is routinely exploited [34]. Similarly, a sufficient number of nanoscale structural heterogeneities in MGs facilitate BMG composites with superior mechanical properties and present a big potential for future studies.

Declaration of Competing Interest

The author declare that there is no conflict of interest.

Acknowledgments

This work was funded by the Austrian Academy of Sciences and the Austrian Science Fund (FWF): I1309, Y1236-N37. Work at the Molecular Foundry was supported by the Office of Science, Office of Basic Energy Sciences, of the U.S. Department of Energy under Contract No. DE-AC02-05-CH11231. Additional support was provided through the European Research Council under the ERC Advanced Grant INTELHYB (grant ERC-2013-ADG-340025). We would like to thank T. Gemming for technical assistance and S. Pauly and H.P. Karnthaler for stimulating discussions.

Author contributions

C.G. carried out the *in situ* deformation experiments. D.B. prepared the BMG specimens including the post-processing treatments. All authors contributed to the analysis and discussion of the results and to the writing of the manuscript.

The datasets analysed during the current study are available from the corresponding author on reasonable request.

Appendix A. Supplementary material

Supplementary data to this article can be found online at https://doi.org/10.1016/j.matdes.2021.109970.

References

[1] M.F. Ashby, A.L. Greer, Scr. Mater. 54 (2006) 321.
[2] C.A. Schuh, T.C. Hufnagel, U. Ramamurty, Acta Mater. 55 (2007) 4067.
[3] M. Hasan, J. Schroers, G. Kumar, Nano Lett. 15 (2015) 963.
[4] J. Li, G. Doubek, L. McMillon-Brown, A.D. Taylor, Adv. Mater. (2019) 31, https://doi.org/10.1002/adma.201802120.
[5] M. Chen, NPG Asia Mater. 3 (2011) 82. https://doi.org/10.1038/asiamat.2011.30.
[6] J. Pan, Y.X. Wang, Q. Guo, D. Zhang, A.L. Greer, Y. Li, Nat. Commun. (2018) 9, https://doi.org/10.1038/s41467-018-02943-4.
[7] C. Ebner, B. Escher, C. Gammer, J. Eckert, S. Pauly, C. Rentenberger, Acta Mater. 160 (2018) 147.
[8] G. Kumar, A. Desai, J. Schroers, Adv. Mater. 23 (2011) 461.
[9] H. Guo, P.F. Yan, Y.B. Wang, J. Tan, Z.F. Zhang, M.L. Sui, E. Ma, Nat. Mater. 6 (2007) 735.
[10] D. Şopu, A. Foroughi, M. Stoica, J. Eckert, Nano Lett. 16 (2016) 4467.
[11] Z. Liu, R. Li, G. Liu, K. Song, S. Pauly, T. Zhang, J. Eckert, AIP Adv. 2 (2012) 032176.
[12] D.C. Hofmann, J. Suh, A. Wiest, G. Duan, M. Lind, M.D. Demetriou, W.L. Johnson, Nature 451 (2008) 1085.
[13] J. Qiao, H. Jia, P.K. Liaw, Mater. Sci. Eng. R 100 (2016) 1.
[14] Y. Wu, Y. Xiao, G. Chen, C.T. Liu, Z. Lu, Adv. Mater. 22 (2010) 2770.
[15] S.S.S. Chen, H.R.R. Zhang, I. Todd, Scr. Mater. 72–73 (2014) 47.
[16] M. Chen, A. Inoue, W. Zhang, T. Sakurai, Phys. Rev. Lett. 96 (2006) 245502.
[17] S. Pauly, S. Gorantla, G. Wang, U. Kühn, J. Eckert, Nat. Mater. 9 (2010) 473.
[18] M. Gao, J. Dong, Y. Huan, Y.T. Wang, W. Wang, Sci. Rep. 6 (2016) 21929.
[19] S. Scudino, B. Jerliu, S. Pauly, K.B. Surreddi, U. Kühn, J. Eckert, Scr. Mater. 65 (2011) 815.
[20] Y. Wang, J. Li, A.V. Hamaza, T.W. Barbee, PNAS 104 (2007) 11155.
[21] G. Wu, S. Balachandran, B. Gault, W. Xia, C. Liu, Z. Rao, Y. Wei, S. Liu, J. Lu, M. Herbig, W. Lu, G. Dehm, Z. Li, D. Raabe, Adv. Mater. (2020) 32, https://doi.org/10.1002/adma.202002619.
[22] B. Sarac, J. Schroers, Nat. Commun. 4 (2013) 2158.
[23] S.W. Lee, M. Jafary-Zadeh, D.Z. Chen, Y.W. Zhang, J.R. Greer, Nano Lett. 15 (2015) 5673.
[24] C. Gammer, C. Ophus, T.C. Pekin, J. Eckert, A.M. Minor, Appl. Phys. Lett. 112 (2018) 171905.
[25] Q.S. Zhang, W. Zhang, G.Q. Xie, A. Inoue, J. Phys. Conf. Ser. 144 (2009) 012031.
[26] A. Warhadpande, B. Jalalahmadi, T. Slack, F. Sadeghi, Int. J. Fatigue 32 (2010) 685.
[27] Q. Zhang, W. Zhang, A. Inoue, Scr. Mater. 55 (2006) 711.
[28] C. Gammer, B. Escher, C. Ebner, A.M. Minor, H.P. Karnthaler, J. Eckert, S. Pauly, C. Rentenberger, Sci. Rep. 7 (2017) 44903.
[29] B. Escher, U. Kühn, J. Eckert, C. Rentenberger, S. Pauly, Mater. Sci. Eng. A 673 (2016) 90.
[30] Y. Liu, J.J. Blandin, M. Suery, G. Kapelski, Mater. Charact. 70 (2012) 8.
[31] S. Jiang, H. Wang, Y. Wu, X. Liu, H. Chen, M. Yao, B. Gault, D. Ponge, D. Raabe, A. Hirata, M. Chen, Y. Wang, Z. Lu, Nature 544 (2017) 460.
[32] E. Clouet, L. Laé, T. Épicier, W. Lefebvre, M. Nastar, A. Deschamps, Nat. Mater. 5 (2006) 482.
[33] V. Radmilovic, C. Ophus, E.A. Marquis, M.D. Rossell, A. Tolley, A. Gautam, M. Asta, U. Dahmen, Nat. Mater. 10 (2011) 710.
[34] W. Gayle, M. Goodway, Science 266 (1994) 1015. http://dx.doi.org/10.1126/science.266.5187.1015.
[35] C.A. Volkert, A. Donohue, F. Spaepen, J. Appl. Phys. 103 (2008) 083539.
[36] K.K. Song, S. Pauly, B.A. Sun, J. Tan, M. Stoica, U. Kühn, J. Eckert, AIP Adv. 3 (2013) 012116.
[37] C. Brandl, T.C. Germann, A. Misra, Acta Mater. 61 (2013) 3600.
[38] B. Cheng, J.R. Trelewicz, Acta Mater. 117 (2016) 293.
[39] J. Fan, W. Rao, J. Qiao, P.K. Liaw, D. Şopu, D. Kiener, J. Eckert, G. Kang, Y. Wu, J. Mater. Sci. Technol. 50 (2020) 192.
[40] C. Ebner, J. Rajagopalan, C. Lekka, C. Rentenberger, Acta Mater 181 (2019) 148.
[41] J. Eckert, J. Das, S. Pauly, C. Duhamel, Adv. Engng Mater. 9 (2007) 443.
[42] X.L. Fu, Y. Li, C.A. Schuh, Scr. Mater. 56 (2007) 617.
[43] R.L. Narayan, P.S. Singh, D.C. Hofmann, N. Hutchinson, K.M. Flores, U. Ramamurty, Acta Mater. 60 (2012) 5089.
[44] T. Brink, M. Peterlechner, H. Rösner, K. Albe, G. Wilde, Phys. Rev. Appl. 5 (2016) 5.
[45] D. Şopu, C. Soyarslan, B. Sarac, S. Bargmann, M. Stoica, J. Eckert, Acta Mater. 106 (2016) 199.